



ISTITUTO NAZIONALE DI RICERCA METROLOGICA Repository Istituzionale

On the possibility to detect quantum correlation regions with the variable optimal measurement angle

This is the author's submitted version of the contribution published as:

Original

On the possibility to detect quantum correlation regions with the variable optimal measurement angle / Moreva, E.; Gramegna, Marco; Yurischev, Mikhail A.. - In: THE EUROPEAN PHYSICAL JOURNAL. D, ATOMIC, MOLECULAR, OPTICAL AND PLASMA PHYSICS. - ISSN 1434-6079. - 73:(2019), p. 68. [10.1140/epjd/e2019-90451-3]

Availability:

This version is available at: 11696/61191 since: 2021-01-29T15:14:46Z

Publisher:

Springer

Published

DOI:10.1140/epjd/e2019-90451-3

Terms of use:

This article is made available under terms and conditions as specified in the corresponding bibliographic description in the repository

Publisher copyright

SPRINGER

Copyright © Springer. The final publication is available at link.springer.com

(Article begins on next page)

On the possibility to detect quantum correlation regions with the variable optimal measurement angle

Ekaterina V. Moreva^{1a}, Marco Gramegna¹, and Mikhail A. Yurischev²

¹ Istituto Nazionale di Ricerca Metrologica, strada delle Cacce 91, 10135 Torino, Italy

² Institute of Problems of Chemical Physics of the Russian Academy of Sciences, 142432 Chernogolovka, Moscow Region, Russia

Revised version: date 14/01/2019

Abstract. Quantum correlations described by quantum discord and one-way quantum deficit can contain ordinary regions with *constant* (i.e., universal) optimal measurement angle 0 or $\pi/2$ with respect to the z -axis and regions with a *variable* (state-dependent) angle of the optimal measurement. The latter regions which are absent in the Bell-diagonal states are very tiny for the quantum discord and cannot be observed experimentally due to various imperfections on the preparation and measurement steps of the experiment. On the contrary, for the one-way quantum deficit we succeeded in getting the special two-qubit X states which seem to allow one to reach all regions of quantum correlation exploiting available quantum optical techniques. These states give possibility to deep investigation of quantum correlations and related optimization problems at new region and its boundaries. In the paper, explicit theoretical calculations applicable to one-way deficit are reported, together with the design of the experimental setup for generating such selected family of states; moreover, there are presented numerical simulations showing that the most inaccessible region with the intermediate optimal measurement angle may be resolved experimentally.

PACS. 03.67.-a Quantum information – 89.70.Cf Entropy and other measures of information – 42.50.Xa Optical tests of quantum theory

1 Introduction

Quantum correlations lie at the heart of quantum information science and technology. Many kinds of quantum correlations have been introduced so far and now their properties are scrupulously analyzed both theoretically and experimentally. Among quantumness quantifiers beyond quantum entanglement, relevant places in the scale of importance are occupied respectively by quantum discord and quantum work (information) deficit [1, 2, 3, 4, 5].

The quantum discord Q for a bipartite system AB is defined as the minimum difference between the quantum generalizations of symmetric (I) and asymmetric (J) forms of classical mutual information: $Q = \min_{\{\Pi_k\}} (I - J)$, where $\{\Pi_k\}$ is the measurement performed on one of the two subsystems [6, 7] (see also [8] in this regard). The quantum discord is always non-negative, equals zero for the classically correlated states, and coincides with the quantum entanglement for the pure states. However, discord and entanglement exhibit essentially different behavior even for the simplest mixed states — the Werner and Bell-diagonal ones (see, e.g. [9, 10]). Note that discord is not a symmetric quantity and in general it depends on which subsystem the local measurement was performed.

A value of quantum discord for two-qubit systems can vary from zero to one bit.

The quantum work deficit is a measure of quantum correlation based on thermodynamics. It was defined firstly by Oppenheim et al. [11] as the difference between the work \mathcal{W} which can be extracted from a heat bath using operations on the entire quantum system and the largest amount of work W drawn from the same heat bath by manipulating only the local parts of composite system; in other words, the work deficit Δ is the amount of potential work which cannot be extracted under local operations and classical communication (LOCC) because of quantum correlations [11, 12, 13]. Several forms of deficit exist, depending on the type of communication allowed between parts A (Alice) and B (Bob). For example, let us consider the case in which the bipartite state ρ_{AB} is shared by Alice and Bob: if Bob performs a single von Neumann measurement on his local subsystem and uses classical communication to send the resulting state to Alice, when she extracts the maximum amount of work W from the new entire state, then the dimensionless quantity $\Delta = \min_{\{\Pi_k\}} (\mathcal{W} - W) / k_B T$ is called the one-way quantum deficit (T is the temperature of the common bath and k_B is Boltzmann's constant). In spite of quite different conceptual sources, the one-way deficit and discord coincide in considerably more general cases than entanglement. They

^a corresponding author: ekaterina.moreva@gmail.com

are the same for the Bell-diagonal states and even for the two-qubit X states¹ with zero Bloch vector for one qubit if the local measurement is performed on this qubit [14]. On the other hand, these quantum correlations exhibit, generally speaking, different quantitative and qualitative behavior in more general cases.

Due to the optimization procedure entering in quantum correlation definitions, evaluation of quantum discord and deficit entails great difficulties even for the two-qubit systems. Up to the present, closed analytical formula for the quantum discord has been derived only for a particular class of X states, namely for the Bell-diagonal states [15]. Since the one-way deficit is identical to the discord in this case, one automatically possesses the closed analytical expression for the former quantity.

An attempt to extend the success of Luo [15] to the arbitrary X states was undertaken in 2010 by Ali, Rau, and Alber [16]. Unfortunately, the authors decided that the extreme values of parameters which characterize the von Neumann measurement were attained for discord only at their endpoints. Shortly after, however, the counterexamples of X density matrices have been given which demonstrate a measurement-dependent discord minimum inside the interval of measurement parameters [17,18]. Thus, the analytic formula of Ref. [16] is incorrect in general.

At that time it was also established that for the general two-qubit X states the optimization of discord over the projectors $\{\Pi_k(\theta, \varphi)\}$ can be worked out exactly over the azimuthal angle φ but one optimization procedure, in the polar angle $\theta \in [0, \pi/2]$, remains relevant [19,20,21] (see also [22]). As a result, a pessimistic verdict has been made: “For general two-qubit X states quantum discord cannot be evaluated analytically” [23].

Definite optimism was restored in Refs. [24,25,26], where it has been observed that the formula for calculating the quantum discord of general two-qubit X states has, in any event, a piecewise-analytical-numerical (semianalytical) form

$$Q = \min\{Q_0, Q_{\theta^*}, Q_{\pi/2}\}. \quad (1)$$

Here the subfunctions (branches) Q_0 and $Q_{\pi/2}$ are the analytical expressions (corresponding to the discord with optimal measurement angles 0 and $\pi/2$, respectively) and only the third branch Q_{θ^*} requires one-dimensional searching of the optimal state-dependent measurement angle $\theta^* \in (0, \pi/2)$ if, of course, the interior global extremum exists.

Thus, the total domain of definition for the discord function consists of subdomains each one corresponding to the own branch (phase or fraction - in physical language) separated by strong boundaries. Equations for such boundaries have been proposed in Refs. [24,25,26]. The equations for 0- and $\pi/2$ -boundaries separating respectively the Q_0 and $Q_{\pi/2}$ regions with the Q_{θ^*} one are written as

$$Q''(0) = 0, \quad Q''(\pi/2) = 0. \quad (2)$$

Here $Q''(0)$ and $Q''(\pi/2)$ are the second derivatives of the measurement-dependent discord function $Q(\theta)$ with respect to θ at the endpoints $\theta = 0$ and $\pi/2$, correspondingly. The equations (2) are based on the unimodality hypothesis for the function $Q(\theta)$ and bifurcation mechanism of appearance of the extremum inside the interval $(0, \pi/2)$. The equations are confirmed now for different subclasses of X states [26,27].

Very similar situation takes place for the one-way quantum deficit of two-qubit X states [28,29,30]. This quantity is given as

$$\Delta = \min\{\Delta_0, \Delta_{\vartheta}, \Delta_{\pi/2}\}, \quad (3)$$

where the branches Δ_0 and $\Delta_{\pi/2}$ are again known in the analytical form while the third branch Δ_{ϑ} requires to perform numerical minimization to obtain state-dependent minimizing polar angle $\vartheta \in (0, \pi/2)$. However the measurement-dependent deficit $\Delta(\theta)$ can exhibit now the bimodal behavior that in turns can lead additionally to the new mechanism of formation of a boundary between the phases, namely via finite jumps of optimal measured angle from the endpoint to the interior minimum or vice versa [29,30].

The analysis performed shows that the discordant region Q_{θ^*} is very narrow. It is characterized by the linear sizes of order 10^{-4} , leading to the fantastically high fidelity² between the boundary states: $F = 99.999998\%$ [27]. Moreover, the volume of Q_{θ^*} -region is 0.08% of total volume of the domain of definition [27]. The latter agrees approximately with the estimation obtained by Monte-Carlo simulations [31] equivalent to 0.03%. Thus, these parameters are unfavorable and exclude any possibility to observe now the exotic Q_{θ^*} -region experimentally.

On the other hand, the analogous regions Δ_{ϑ} of one-way quantum deficit can achieve the sizes comparable to those of the regions Δ_0 and $\Delta_{\pi/2}$, therefore inspiring the possibility that an insight into the considered region can be obtained experimentally.

The aim of present paper is to select suitable quantum states showing the widest possible regions with the variable intermediate optimal measurement angle, to perform for them numerical simulations, and to give a response about the possibility to resolve such regions using contemporary optical apparatus.

Our aspiration to experimentally detect the new regions (phases) of quantum correlations is motivated by the following. First, this is a study of properties of quantum correlations which are absent in the Bell-diagonal states. In particular, the observation of continuous and smooth transitions between the phases which manifest in higher derivatives with respect to the state parameters. Secondly, the fact that the state lies in the region of the variable optimal measurement allows us to estimate the value of quantum correlation via the shift of the angle.

Third, the regions of quantum states with the intermediate optimal measurement angle are rather surprising

¹ A matrix having non-zero entries only along the diagonal and anti-diagonal is called the X one because it looks like the letter “X”.

² The fidelity of two quantum states, F , leads to the Bures distance, d_B , between the same states through the relation $d_B = [2(1 - \sqrt{F})]^{1/2}$.

because the most practical constrained optimization problems in the natural sciences have an optimal solution at the boundary. (See, e.g., [32]: “Real life optimization problems often involves one or more constraints and in most cases, the optimal solutions to such problems lie on constraint boundaries.”) However this expectation can lead to incorrect results like in [16].

In the following sections, a suitable candidate of quantum state is given, its properties are described in detail, a scheme of optical setup is considered and the expected results are discussed. Finally, in the last section, a brief conclusion is given.

2 Theoretical results

We begin with the theoretical description of the problem under question.

2.1 One-way deficit estimation

The maximum amount of useful work that can be extracted from a system in the state ρ is given as [11,12,13] (see also [1,2,3])

$$w = k_B T (\log d - S(\rho)), \quad (4)$$

where $S(\rho) = -\text{tr}(\rho \log \rho)$ is the entropy of state ρ and d the dimension of Hilbert space in which the density operator ρ acts. Applying this general relation to the states before and after Bob’s measurement it is possible to obtain the following equation for the one-way deficit

$$\Delta = \min_{\{\Pi_k\}} S(\tilde{\rho}_{AB}) - S(\rho_{AB}), \quad (5)$$

where

$$\tilde{\rho}_{AB} \equiv \sum_k p_k \rho_{AB}^k = \sum_k (\mathbf{I} \otimes \Pi_k) \rho_{AB} (\mathbf{I} \otimes \Pi_k)^+ \quad (6)$$

is the weighted average of post-measured states

$$\rho_{AB}^k = \frac{1}{p_k} (\mathbf{I} \otimes \Pi_k) \rho_{AB} (\mathbf{I} \otimes \Pi_k)^+ \quad (7)$$

with the probabilities

$$p_k = \text{Tr}(\mathbf{I} \otimes \Pi_k) \rho_{AB} (\mathbf{I} \otimes \Pi_k)^+. \quad (8)$$

Thus, the one-way quantum deficit equals the minimal increase of entropy after a von Neumann measurement on one party of the bipartite system ρ_{AB} .

It is clear from Eq. (5) that the main problem is to find the post-measurement entropy, because the pre-measurement one, i.e. $S(\rho_{AB})$, does not depend on the measuring angle and hence plays a role of a trivial constant shift. Therefore, below we will stress attention mainly on the $S(\tilde{\rho}_{AB})$.

Generally the one-way deficit, as the quantum discord, is asymmetric quantity under replacement of the measured subsystem, however we avoid such cases in our work.

Notice that the map $\rho_{AB} \mapsto \tilde{\rho}_{AB}$ defined by Eq. (6) can be interpreted as non-selective measurement (see, e.g., the textbook [33]) because not the individual measurement outcomes are recorded but only the statistics of outcomes is known. (Note in passing that the quantum discord is based on selective measurements.) Moreover, this map has a form of quantum operation and therefore the one-way deficit has the operational significance beyond entanglement.

It arises a question: how to determine the entropy of some quantum state ρ experimentally? In order to get the thermodynamic entropy one measures the heat capacity of the given sample, takes the ratio of heat capacity to the temperature and then integrates this ratio with respect to the temperature. In the quantum case, in line with the measurement propositions [34,35], direct way is to take the entropy operator $-\log \rho$ [36] or the density one ρ as an observable. However, it is not known how to experimentally realize the projectors $|\lambda_k\rangle\langle\lambda_k|$, where $|\lambda_k\rangle$ are the eigenvectors of above operators. Instead, one can first restore the quantum state ρ through a tomographic reconstruction in the computational basis (i.e., find the numerical values for all entries of the density matrix), solve eigenvalue problem for this matrix on a computer, and then calculate the quantum entropy via the relation $S(\rho) = -\sum_i \lambda_i \log \lambda_i$ with λ_i being the eigenvalues of ρ [37]. It is the way that we use in the present paper.

There is, of course, the radical way to obtain the one-way deficit without performing any local measurements at all (as it is usually made to get the quantum entanglement; say, [38]). Indeed, since the full tomography is needed to find the entropy of pre-measurement state, one can use the digital representation of ρ_{AB} to numerically perform the required local measurement, compute the minimized post-measurement entropy, and finally arrive at the value of one-way deficit Δ . We keep in mind this possibility and will compare both approaches in the real experimental work. Both possibilities have their pluses and minuses. If the local measurement is performed in analog way, then the numerical calculations are simplified, moreover we prefer to consider “real” measurements with their imperfections for the simulation of the experiment.

To continue our consideration one should specify the quantum state.

2.2 Initial quantum state ρ_{AB}

Focussing on two-qubit systems, to this date, phase diagrams for the quantum discord and one-way deficit have been studied in detail for the three-parameter subclass of two-qubit X states [27,30]. This allows us to choose the suitable state to examine it in an experiment.

From the available variety of states, we consider here the maximally simple (but non-trivial) one-parameter state

$$\rho_{AB} = q|\Phi^+\rangle\langle\Phi^+| + (1-q)|01\rangle\langle 01|, \quad (9)$$

where $|\Phi^+\rangle = (|00\rangle + |11\rangle)/\sqrt{2}$. This state in a Bloch form is written as

$$\rho_{AB} = 4^{-1}[\mathbf{I} \otimes \mathbf{I} + (1-q)(\sigma_z \otimes \mathbf{I} - \mathbf{I} \otimes \sigma_z)]$$

$$+q(\sigma_x \otimes \sigma_x - \sigma_y \otimes \sigma_y) + (2q - 1)\sigma_z \otimes \sigma_z], \quad (10)$$

where σ_α ($\alpha = x, y, z$) is the vector of the Pauli matrices. The given state will show the obvious symmetry under permutations of particles ($A \leftrightarrow B$) after performing the local unitary (orthogonal) transformation $U = I \otimes \sigma_x$ which does not change any of the quantum correlations. Lastly, the density matrix of chosen state ρ_{AB} in explicit form is given by

$$\rho_{AB} = \begin{pmatrix} q/2 & 0 & 0 & q/2 \\ 0 & 1-q & 0 & 0 \\ 0 & 0 & 0 & 0 \\ q/2 & 0 & 0 & q/2 \end{pmatrix}. \quad (11)$$

Let us consider now the class of states (9) showing the maximum amount of entanglement investigated in Refs. [39, 40, 41]. It is remarkable that the authors [39] were able to achieve the fidelity $F \geq 99\%$. Later the discordant features of the above state were discussed in Ref. [42]. Notice that the quantum discord for the state (9) is defined by the optimal measurement angle $\theta^* = \pi/2$ in the whole interval of parameter q and hence the discord has here no regions with the variable optimal measurement angles.

In this paper we focus on the one-way deficit. According to Eq. (5), to find this quantity, one should first calculate the pre- and post-measurement entropies — $S(\rho_{AB})$ and $S(\tilde{\rho}_{AB})$, respectively. For this purpose, we find the corresponding eigenvalues.

Eigenvalues of matrix (11) equal

$$\lambda_1 = q, \quad \lambda_2 = 1 - q, \quad \lambda_3 = \lambda_4 = 0. \quad (12)$$

Owing to the non-negativity requirement for any density matrix, one obtains that the domain of definition for the parameter (argument) q is restricted by the condition

$$0 \leq q \leq 1. \quad (13)$$

The quantity q may be interpreted as a concentration of Bell-diagonal state in the two-component mixture (9).

Using Eq. (12) one gets the pre-measured entropy function

$$S(q) \equiv S(\rho_{AB}) = -q \log q - (1 - q) \log(1 - q). \quad (14)$$

This is exactly the binary entropy and its value can vary from zero to one bit.

2.3 Post-measurement state $\tilde{\rho}_{AB}$

Since ρ_{AB} is the two-qubit state, then Π_k in Eq. (6) are the two projectors ($k = 0, 1$)

$$\Pi_k = V \pi_k V^+, \quad (15)$$

where $\pi_k = |k\rangle\langle k|$ and transformations $\{V\}$ belong to the special unitary group SU_2 . Rotations V are parametrized by two angles θ and φ (polar and azimuthal, respectively):

$$V = \begin{pmatrix} \cos(\theta/2) & e^{i\varphi} \sin(\theta/2) \\ \sin(\theta/2) & -e^{i\varphi} \cos(\theta/2) \end{pmatrix} \quad (16)$$

with $0 \leq \theta \leq \pi$ and $0 \leq \varphi < 2\pi$.

Performing the necessary calculations it is possible to get the eigenvalues of the density matrix $\tilde{\rho}_{AB}$:

$$A_{1,2} = \frac{1}{4} [1 + (1 - q) \cos \theta \pm \{[1 - q + (1 - 2q) \cos \theta]^2 + q^2 \sin^2 \theta\}^{1/2}] \quad (17)$$

$$A_{3,4} = \frac{1}{4} [1 - (1 - q) \cos \theta \pm \{[1 - q - (1 - 2q) \cos \theta]^2 + q^2 \sin^2 \theta\}^{1/2}].$$

It is seen that the azimuthal angle φ has dropped out from the given expressions. This is due to the fact that one pair of anti-diagonal entries of the density matrix (11) vanishes. Using Eqs. (17) we arrive at the post-measured entropy (entropy after measurement)

$$\tilde{S}(\theta; q) \equiv S(\tilde{\rho}_{AB}) = h_4(A_1, A_2, A_3, A_4), \quad (18)$$

where $h_4(x_1, x_2, x_3, x_4) = -\sum_{i=1}^4 x_i \log x_i$, with the additional condition $x_1 + x_2 + x_3 + x_4 = 1$, is the quaternary entropy function. Notice that function \tilde{S} of argument θ is invariant under the transformation $\theta \rightarrow \pi - \theta$ therefore it is enough to consider the values for which $\theta \in [0, \pi/2]$.

It is worth noticing that since the post-measurement state is needed only to find its entropy, which is invariant under any unitary transformations, one can transfer the rotations V from the measurement operators (projectors) on the state ρ_{AB} :

$$\tilde{\rho}_{AB} \mapsto \tilde{\rho}'_{AB} = (I \otimes \pi_0) \cdot [(I \otimes V^+) \rho_{AB} (I \otimes V)] \cdot (I \otimes \pi_0) + (I \otimes \pi_1) \cdot [(I \otimes V^+) \rho_{AB} (I \otimes V)] \cdot (I \otimes \pi_1) \quad (19)$$

and in this case $S(\tilde{\rho}_{AB}) = S(\tilde{\rho}'_{AB})$. It means that we may firstly rotate the state (e.g., with a half-wave plate) and then perform two orthogonal projections of the rotated state in the *initial* computational basis.

2.4 Behavior of post-measurement entropy

We describe here specific properties of post-measurement entropy which will be needed for performing the experiment. In other words, we shall try to supply experimentalists with technological maps suitable in the work.

Equations (14), (17), and (18) define the measurement-dependent (non-optimized) one-way deficit function $\Delta(\theta) = \tilde{S}(\theta) - S$. Direct calculations show that for every choice of model parameter q the function $\tilde{S}(\theta)$ and hence $\Delta(\theta)$ possess an important property, namely their first derivatives with respect to θ identically equal to zero at both endpoints $\theta = 0$ and $\theta = \pi/2$:

$$\tilde{S}'(0) = \Delta'(0) \equiv 0, \quad \tilde{S}'(\pi/2) = \Delta'(\pi/2) \equiv 0. \quad (20)$$

From Eqs. (17) and (18) we get the expressions for the post-measurement entropy at the endpoint $\theta = 0$,

$$\tilde{S}_0(q) = -(1 - q) \log(1 - q) - q \log(q/2), \quad (21)$$

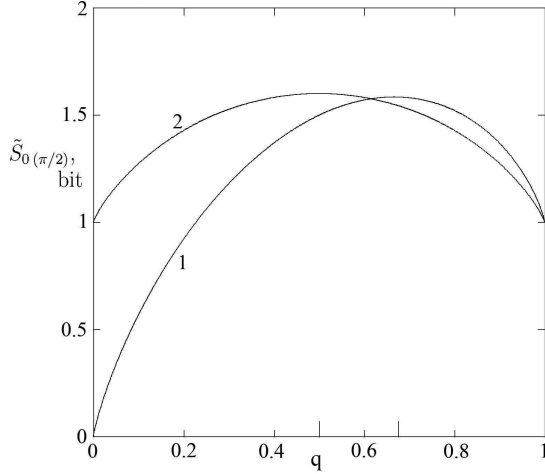


Fig. 1. Dependencies $\tilde{S}_0(q)$ (curve 1) and $\tilde{S}_{\pi/2}(q)$ (curve 2). Longer bars mark the position of interval $[0.5, 0.67515]$

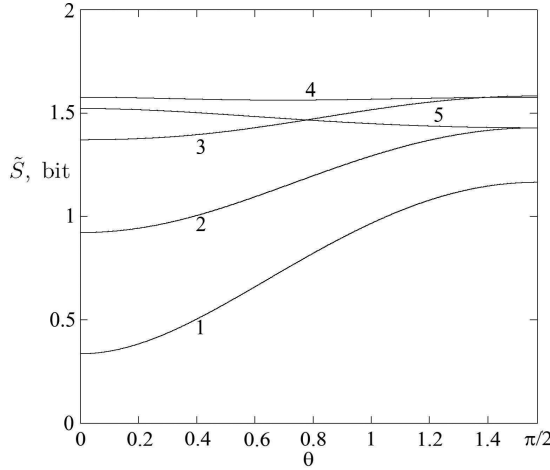


Fig. 2. Post-measurement entropy \tilde{S} vs θ by $q = 0.05$ (1), 0.2 (2), 0.4 (3), 0.6155 (4), and 0.8 (5)

and at the second endpoint $\theta = \pi/2$:

$$\tilde{S}_{\pi/2}(q) = \log 2 + h((1 + \sqrt{(1-q)^2 + q^2})/2), \quad (22)$$

where $h(x) = -x \log x - (1-x) \log(1-x)$ is the Shannon binary entropy function. The behavior of functions $\tilde{S}_0(q)$ and $\tilde{S}_{\pi/2}(q)$ is depicted in Fig. 1. The local maxima of these functions lie at $q = 2/3$ and $1/2$, and equal $\log_2 3 \approx 1.58496$ bits and $\frac{1}{4}[10 - \sqrt{2} \log_2(3 + 2\sqrt{2})] \approx 1.60088$ bits, respectively. The function $\tilde{S}_{\pi/2}(q)$ is symmetric under the replacement $q \rightarrow 1 - q$. The curves 1 and 2 intersect at the point $(0.61554, 1.57667)$.

Together with Eq. (14), the relations (21) and (22) supply us with explicit expressions for the one-way deficit at the endpoints: $\Delta_0 = \Delta(0)$ and $\Delta_{\pi/2} = \Delta(\pi/2)$. In particular, $\Delta_0 = q \log 2$ ($= q$ bits).

At the 0- and $\pi/2$ -boundaries, the second derivatives of the deficit and the post-measurement entropy are:

$$\Delta''(0) = 0 \quad \text{and} \quad \Delta''(\pi/2) = 0 \quad (23)$$

$$\tilde{S}''(0) = 0 \quad \text{and} \quad \tilde{S}''(\pi/2) = 0 \quad (24)$$

will be needed below.

As calculations yield,

$$\tilde{S}''(0) = \frac{1 - 3q + 2q^2}{2 - 3q} \ln \frac{2(1 - q)}{q}. \quad (25)$$

The roots of equation $\tilde{S}''(0) = 0$ are $1/2$ and 1 .

On the other hand, calculations show that the second derivative $\tilde{S}''(\theta)$ with respect to θ at $\theta = \pi/2$ equals

$$\begin{aligned} \tilde{S}''(\pi/2) = & \frac{q^2}{2r^3} [r^2 - (1 - 2q)^2] \ln \frac{1 + r}{1 - r} \\ & - \frac{(1 - q)^2}{1 - r^2} [1 - 2(1 - 2q)(1 - \frac{1 - 2q}{2r^2})], \end{aligned} \quad (26)$$

where

$$r = \sqrt{(1 - q)^2 + q^2}. \quad (27)$$

The results of numerical solution of the equation $\tilde{S}''(\pi/2) = 0$ are $q = 0.67515$ and again an uninteresting root equaled 1 . Thus, the region with the interior optimal measurement angle can exist only when $q \in (0.5, 0.67515)$.

Let us consider now the behavior of post-measured entropy for different values of parameter q in the segment $[0, 1]$. The values of entropy in two-qubit systems can vary from zero to two bits. Figure 2 shows the the behavior of post-measurement entropy upon the measurement angle θ by different values of parameter q . The curves $\tilde{S}(\theta)$ for $q \leq 0.5$ have the monotonically increasing behavior and here the optimal measurement angle is constant equaling zero. The relative difference between values of entropy at endpoints $\theta = 0$ and $\pi/2$ is large and achieves 71%, 35%, and 13% respectively for $q = 0.05$, 0.2 , and 0.4 (see Fig. 2). Conversely, the curves of post-measurement entropy exhibit the monotonically decreasing dependence for $q > 0.67515$. For example, the relative difference $(\tilde{S}(0) - \tilde{S}(\pi/2))/\tilde{S}(0)$ equals 6% for $q = 0.8$ (see again Fig. 2). So, the presented estimates are large enough and therefore allow to hope that the effect of correlation-function transition from the optimal measurement angle zero to $\pi/2$ can be observed in an experiment.

Let us discuss now the behavior of post-measurement entropy in the intermediate region $0.5 < q < 0.67515$. Figure 3 shows the evolution of behavior of the post-measured entropy $\tilde{S}(\theta)$ with respect to parameter q . The curve presents a monotonic increase when the parameter q varies from zero to $q = 1/2$. At the point $q = 1/2$, as visible in Fig. 3(a), a bifurcation of the minimum at $\theta = 0$ occurs. In the range $0.5 < q < 0.67515$, the curve $\tilde{S}(\theta)$ reaches, as shown in Figs. 3(b) and (c), the interior minimum. So, the region with variable optimal angle ϑ takes up a part $0.17515 \approx 17.5\%$ on the section $[0, 1]$ of q axis, and the fidelity between the states at bound points $q = 0.5$ and $q = 0.67515$ equals $F = 96.8\%^3$. The position of such a local minimum ϑ smoothly moves from zero to $\pi/2$ (see again the curves in Figs. 3(b) and (c)).

³ Note for comparison that experimenters achieve now the values of fidelity $F = 99.8(2)\%$ [38], $99.8(1)\%$ [43], and 99.998% [44].

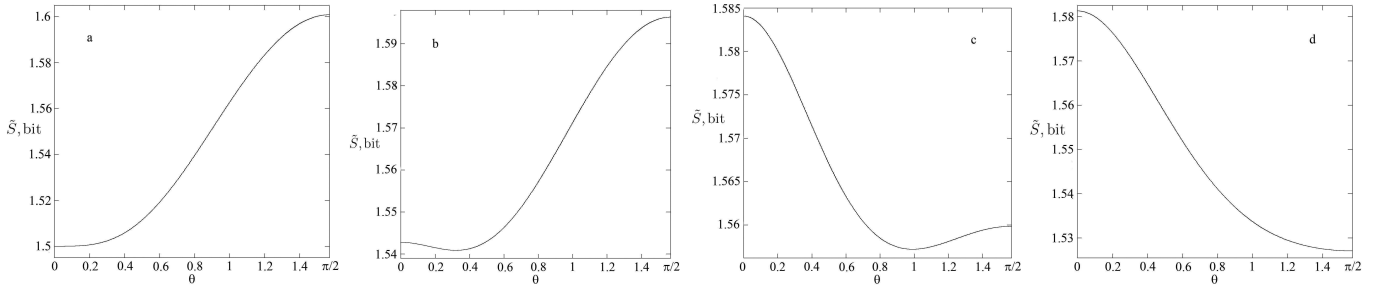


Fig. 3. Post-measurement entropy \tilde{S} vs θ by $q = 0.5$ (a), 0.55 (b), 0.65 (c), and 0.7 (d)

The interior minimum of post-measurement entropy is best observed when the values of \tilde{S}_0 and $\tilde{S}_{\pi/2}$ equal to one another. This occurs (see Fig. 1) at the point $q = 0.61554$ for which $\tilde{S}_0 = \tilde{S}_{\pi/2} = 1.57667$ bits and hence $\Delta_{\pi/2} = \Delta_0 = q = 0.61554$ bit. The given situation is represented in Fig. 4 (cf. with the curve 4 in Fig. 2). Here the minimum lies at the angle $\theta_{min} \equiv \vartheta = 0.6955 \approx 39.8$. Its depth is 0.01397 bit what yields relative corrections to the post-measurement entropy and one-way deficit equalled $\delta\tilde{S} = 0.9\%$ and $\delta\Delta = 2.3\%$, respectively.

Then, at the value of $q = 0.67515$, the system experiences a new hidden sudden transition – from the branch, which is characterized by the continuously changing optimal angle ϑ in the full interval (from 0 to $\pi/2$), to the branch $\tilde{S}_{\pi/2}$ with constant optimal measurement angle equalled $\pi/2$. From here and up to $q = 1$, the curves of post-measured entropy exhibit monotonically decreasing behavior as illustrated in Fig. 3(d).

One should emphasize here that the behavior of the minimized one-way quantum deficit $\Delta = \min_{\theta} \Delta(\theta)$ with respect to the argument q is continuous and smooth. Nevertheless, the function $\Delta(q)$ is a piecewise one,

$$\Delta(q) = \begin{cases} \Delta_0, & 0 \leq q \leq 0.5; \\ \Delta_{\pi/2}, & 0.67515 \leq q \leq 1; \\ \Delta_{\vartheta}, & q \in (0.5, 0.67515), \end{cases} \quad (28)$$

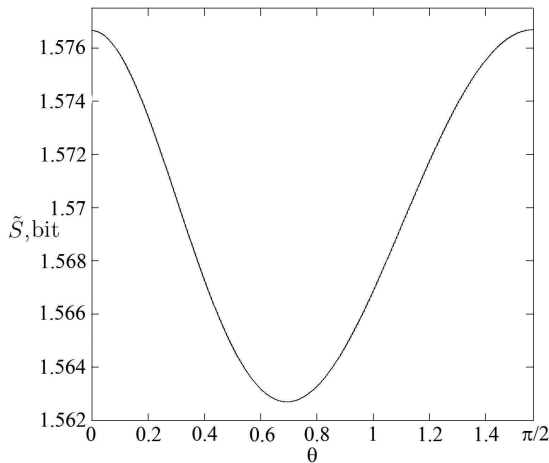


Fig. 4. High-resolved post-measurement entropy \tilde{S} vs θ by $q = 0.6155$

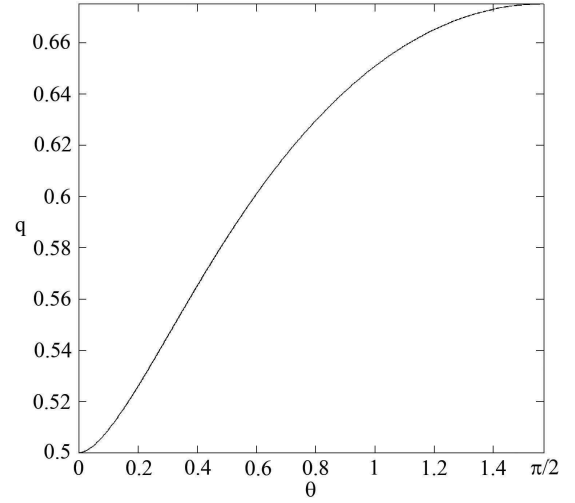


Fig. 5. Concentration of Bell-diagonal state, $q \in [0.5, 0.67515]$, in the mixture (9) as a function of interior optimal measurement angle ϑ .

and therefore presents nonanalyticities at the border points $q = 0.5$ and 0.67515 which manifest themselves in higher derivatives.

The relation of interior optimal measurement on angle ϑ with $q \in [0.5, 0.67515]$ is shown in Fig. 5. The function $q(\vartheta)$ is biunique (one-to-one) and the presented curve allows to estimate the value of parameter q in the mixed quantum state ρ_{AB} . Hence, this can serve as one of possible applications of quantum correlation in practice.

3 Setup and numerical simulations

For testing the theoretical approach, described in the previous sections, we propose a design of an experimental setup allowing to prepare a family of polarization states $\rho_{AB}(9)$ and estimate the post-measured entropy \tilde{S} through the tomographic reconstruction of density matrix. In particular, we suggest to use the well-known method of polarization state preparation via spontaneous parametric down-conversion process (SPDC) [46] and quantum state tomography protocol based on tetrahedral symmetry [47], guaranteeing simple realization and high quality of reconstruction. We intentionally selected commonly used

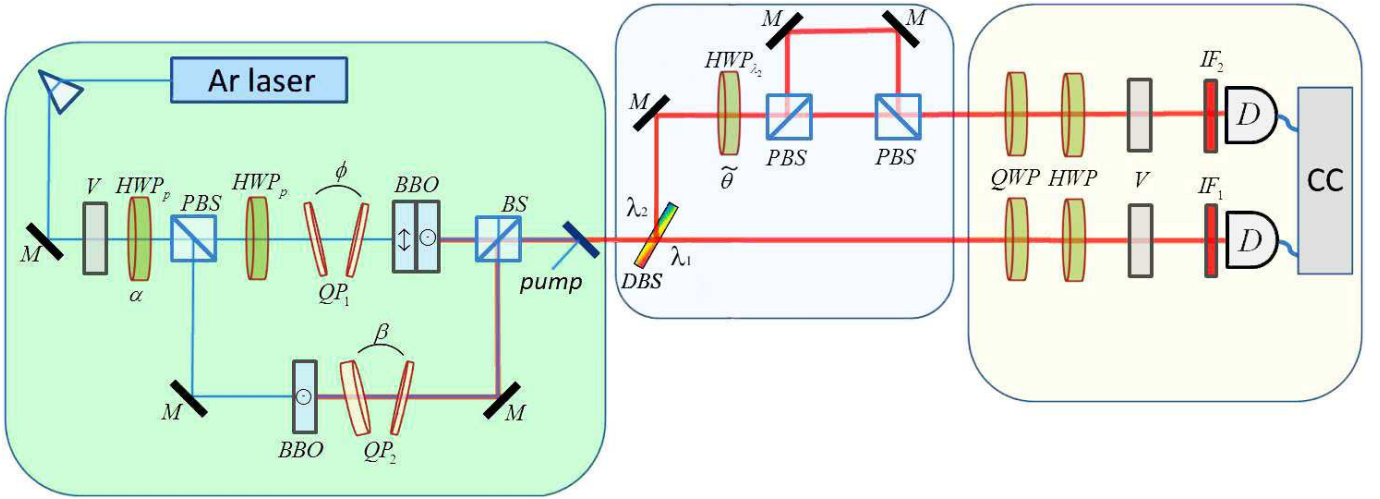


Fig. 6. (Color online) Experimental setup for preparing the initial quantum state and measuring its one-way deficit. The first (green) block prepares the specific quantum states ρ_{AB} defined in (9), the second (blue) block performs local measurements while the third (yellow) block of tomography measures the transformed quantum state $\tilde{\rho}_{AB}$. Ar laser: argon laser with wavelength 351 nm, M: mirror, V: vertical oriented Glan-Thompson prism, BBO: nonlinear barium borate crystals of Type-I, HWP and QWP: half- and quarter-wave plates, QP: (dichroic) quartz plates, BS: beamsplitter, PBS: polarizing beamsplitter, DBS: dichroic beamsplitter (dichroic mirror), IF: interference filter, D: single photon avalanche detectors (SPAD), CC: coincidence circuit

methods to show that the nontrivial behavior of quantum deficit can be observed without requiring specific apparatus.

3.1 Optical setup scheme

The setup is schematically depicted in Fig. 6. A cw argon laser beam at $\lambda = 351$ nm passes through a Glan-Thompson prism (V) with vertical orientation, half-wave plate HWP_p and polarizing beamsplitter (PBS). The HWP_p and PBS serve to control the q parameter in the state ρ_{AB} (9). In the upper arm of non-balanced interferometer the maximum entangled Bell state $|\Phi^+\rangle$ is produced. Two nonlinear type-I BBO crystals, positioned with the planes containing optical axes orthogonal to each other, generate a pair of the basic states $|H_1H_2\rangle, |V_1V_2\rangle$ via collinear, frequency nondegenerated regime of SPDC. The relative phase ϕ between basic states is controlled by two quartz plates QP_1 , while amplitudes are controlled by the half-wave plate HWP_p .

Among th others, and as a practical example, let us suppose that the wavelengths of the collinear downconverted photons are $\lambda_1 = 763$ nm and $\lambda_2 = 650$ nm. In the bottom arm, where the horizontal polarization of the pump is reflected, the second component of the state ρ_{AB} is prepared. We use the technique, suggested in the papers [45,46], to perform the transformation $|V_1V_2\rangle \Rightarrow |H_1V_2\rangle$. This transformation can be achieved by using dichroic wave plates QP_2 , which act separately on the photons with different frequencies and introduce a phase shift of 2π for a vertically polarized photon at 650 nm, a phase shift of π for the conjugated photon at 763 nm. The wave plates are oriented at 45° to the vertical direction. Using

quartz plates as retardation material it is easy to calculate that the thickness of the wave plate operating the transformation should be equal to 1.585 mm or 3.464 mm. The theoretical estimated fidelity is more than 0.998, the difference from unit is related to the imperfection of phase transformation for two photons simultaneously.

Since the result of transformation is extremely sensitive to small variations of thickness, we suggest to use the following method to achieve the desired thickness. Two quartz plates with different thicknesses and with orthogonally oriented optical axes correspond to the action of the quartz wave plate with an effective thickness, equal the difference of the thicknesses of two plates. If then one can tilt these wave plates towards each other by a finite angle β , then the optical thickness of the effective wave plate formed by QP_2 will change, and, at a certain value of β , the desired transformation will be achieved. Ultimately, non-polarizing beamsplitter (BS) mixes the states from the upper and bottom arms of non-balanced interferometer and, as a result, prepares the initial state ρ_{AB} .

The local projective measurements at a variable angle are realized in the (blue) block in Fig. 6. According to Eq. (19) they are implemented only over one of the photon of the pair, so a dichroic beamsplitter (DBS) separates photons with different frequencies into the two spatial modes. In the upper spatial mode a half-wave plate (HWP_{λ_2}) is oriented at the angle $\tilde{\theta}$ [$\tilde{\theta} = \theta/4$ is the angle between the input polarization and the wave plate fast axis, θ is the polar angle in the transformation (16)] and a couple of polarizing beam splitters (PBS), forming a non-balanced interferometer, perform two orthogonal projections at different angles. To obtain the statistical mixture (19) the length difference between the arms of non-balanced interferometer must be larger then the coherence

length of the photons with orthogonal polarization, which for the selected wavelength (λ_2) and a full width at half maximum (FWHM) $\delta\lambda = 3$ nm of the interference filter IF₂ equals $\lambda^2/\delta\lambda \approx 140$ μm .

After the non-selective projective measurement the state was sent to the reconstruction block of the setup (the third (yellow) block in Fig. 6). The post-measured quantity of the entropy (18) at varying angle $\tilde{\theta}$ was numerically calculated through the density matrices of post-measurement state $\tilde{\rho}_{AB}$ using quantum tomography protocols [46]. The projective measurements in each arm to perform the quantum state tomography can be realized by means of a polarization filtering system consisting of a sequence of quarter- and half-wave plates, followed by a polarization prism, which transmits vertical polarization (V). The detection is operated by taking advantage of silicon single-photon avalanche detectors (SPAD). In the case of independent measurement of two qubits the projective measurements can be chosen arbitrarily. We propose quantum state tomography protocol, where projections on the states possess tetrahedral symmetry [47]. There are several works showing that due to the high symmetry such protocol provides a better quality of reconstruction [47, 48, 49]. As alternative, adaptive quantum tomography protocols can be used: in fact, despite these require more complex analysis, they guarantee at the same time the highest quality of state reconstruction [50, 51].

3.2 Numerical simulations

According to the theory, the region with the variable optimal measurement angle is narrow and therefore requires precise quantum state preparation and reconstruction. It is worth to stress that the standard procedure of the state reconstruction from the likelihood equation associates with finite statistics of the registered outcomes (sample size) of an experiment and therefore takes random values [46, 52]. For the state ρ_{AB} we can calculate the statistical distribution of fidelity F for the given sample size.

Usually the quantum tomography protocol can be defined by a so-called instrumental matrix X that has m rows and s columns [53, 54, 55], where s is the Hilbert space dimension and m the number of projections in such space. For every row, i.e. for every projection, there is a corresponding amplitude M_j . This matrix equals:

$$M_j = X_{jl}c_l \quad (j = 1, 2, \dots, m; \quad l = 1, 2, \dots, s), \quad (29)$$

where c_l are the expansion coefficients.

The square of the absolute value of the amplitude defines the intensity of a process, which is the number of events in one second

$$\lambda_j = |M_j|^2. \quad (30)$$

The number of registered events k_j is a random variable exhibiting Poisson distribution, t_j is the time of exposition of the selected row of the protocol and $\lambda_j t_j$ the average value,

$$P(k_j) = \frac{(\lambda_j t_j)^{k_j}}{k_j!} \exp(-\lambda_j t_j). \quad (31)$$

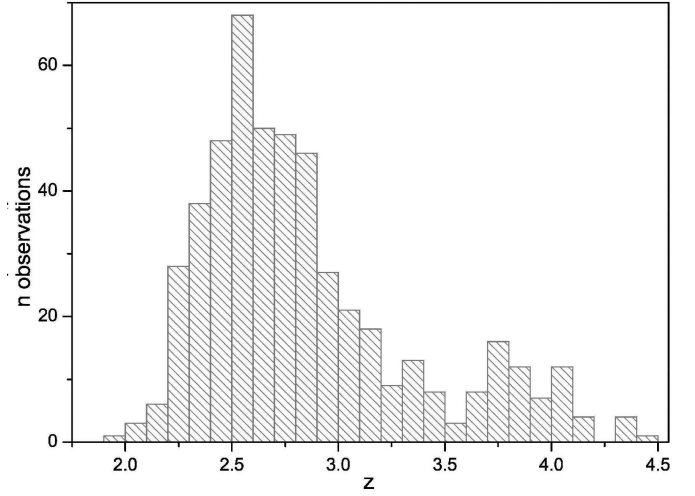


Fig. 7. The universal statistical fidelity loss histogram distribution for 500 numerical experiments. Sample size of each experiment is 10^5

The normalization condition for the protocol defines the total expected number of events n summarized by all rows:

$$\sum_{j=1}^m \lambda_j t_j = n. \quad (32)$$

Equation (32) substitutes the traditional normalization condition for the density matrices, $\text{tr}(\rho) = 1$.

The fidelity achieved now by experimenters has the values $F \geq 99.8\%$ for the given optical states (9) [38, 43, 44], that is why in the numerical experiments testing the universal statistical distribution for fidelity losses we used statistics that guarantees the same fidelity: we numerically generated sets of experimental data and reconstructed 500 states ρ_{AB} ($q = 0.6155$) with sample size around $n = 10^5$ for each state, obtained by performing the maximum-likelihood estimation on random variables of the measured counts according to Poissonian statistics. The estimated average fidelity with absolute error is $F = 0.998 \pm 0.02$. The fluctuations of F can be formally taken into account by introducing the so-called loss of fidelity $1 - F$, which is associated only with statistical errors and does not take into account experimental imperfections. We can also introduce the variable $z = -\log_{10}(1 - F)$, which is the number of digit 9 in the decimal representation of the parameter F (e.g., $z = 3$ corresponds to $F = 0.999$). Figure 7 shows the universal statistical fidelity loss histogram distribution for 500 simulated states ρ_{AB} . The form of the distribution besides sample size depends on the initial state and the used protocol of quantum state reconstruction. In our simulation the tomography protocol based on the states possessing tetrahedral symmetry had been used [47].

For the same sample size we estimated numerically the post-measured entropy for the best observed interior minimum at the point $q = 0.6155$. For each angle $\tilde{\theta}$, which

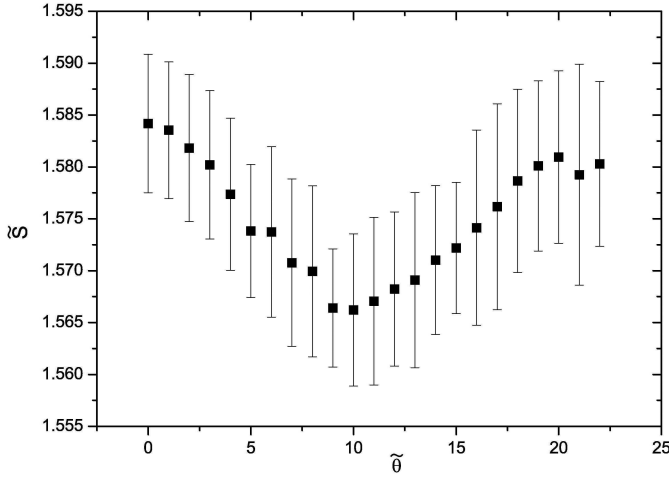


Fig. 8. Post-measurement entropy \tilde{S} vs $\tilde{\theta}$ by $q = 0.6155$ for 100 numerical experiments. Squares are mean values \tilde{S} , bars are standard deviations. Sample size of each experiment is 10^5 . It is clearly seen a minimum of $\tilde{S}(\tilde{\theta})$ near the angle $\tilde{\theta} = 10^\circ$, that is in good agreement with the theoretical prediction shown in Fig. 4

varies from 0° to 22° (with step 1°), a set of 100 density matrices of $\tilde{\rho}_{AB}$ was generated, then eigenvalues were calculated and finally the mean values together with standard deviations of the post-measured entropy \tilde{S} were estimated. The dependence \tilde{S} on $\tilde{\theta}$ is plotted on Fig. 8. The graph shows that with a good experimental accuracy, it is possible to observe the region with the variable optimal measurement angle taking advantage of the proposed setup, even if the corrections to the post-measurement entropy values are small (in the order of 0.9% or less).

4 Conclusion

In this work we have found the specific quantum state (9) with the record wide region of variable optimal measurement angle, presented for it the detailed calculations of entropy after measurement and hence of one-way deficit, and performed the numerical simulation of the proposed experiment.

The described experimental setup opens a possibility to construct universal facilities allowing to measure the one-way deficit of any symmetric (up to local unitary transformation) two-photon quantum states. Moreover, we have considered in detail the preparation of two-component mixture of quantum states which, according to the theory, contains a fraction with the variable optimal measurement angle.

The performed numerical simulations show that the available experimental techniques allows one to investigate a fine structure of quantum correlation domain including the region with the variable optimal measurement angle and opens a way to implement the real physical experiment to study the one-way deficit behavior.

Acknowledgments

One of us (M. Yu.) is grateful to participants of the Seminar of the Quantum Technologies Center of the Lomonosov Moscow State University for fruitful discussion.

5 Author contribution statement

M.Yu. contributed with theoretical calculations of one-way quantum deficit and wrote the theoretical part of the manuscript, E.M. contributed to the experimental setup design, numerical simulation and wrote the experimental part of the manuscript, M.G. helped with experimental setup design and critical revision of the manuscript.

References

1. K. Modi, A. Brodutch, H. Cable, T. Paterek, and V. Vedral, *Rev. Mod. Phys.* **84**, 1655 (2012)
2. A. Streltsov, *Quantum correlations beyond entanglement and their role in quantum information theory* (Springer, Berlin 2015)
3. G. Adesso, T. R. Bromley, and M. Cianciaruso, *J. Phys. A: Math. Theor.* **49**, 473001 (2016)
4. *Lectures on general quantum correlations and their applications*. Edited by F. F. Fanchini, D. O. Soares-Pinto, and G. Adesso (Springer, Berlin 2017)
5. A. Bera, T. Das, D. Sadhukhan, S. S. Roy, A. Sen(De), and U. Sen, *Rep. Prog. Phys.* **81**, 024001 (2018)
6. W. H. Zurek, *Ann. Phys. (Leipzig)* **9**, 855 (2000)
7. H. Ollivier and W. H. Zurek, *Phys. Rev. Lett.* **88**, 017901 (2002)
8. L. Henderson and V. Vedral, *J. Phys. A: Math. Gen.* **34**, 6899 (2001)
9. M. A. Yurishchev, *Phys. Rev. B* **84**, 024418 (2011)
10. E. Moreva, M. Gramegna, and M. A. Yurishchev, *Adv. Sci. Eng. Med.* **9**, 46 (2017); arXiv:1612.04589v1 [quant-ph]
11. J. Oppenheim, M. Horodecki, P. Horodecki, and R. Horodecki, *Phys. Rev. Lett.* **89**, 180402 (2002)
12. M. Horodecki, K. Horodecki, P. Horodecki, R. Horodecki, J. Oppenheim, A. Sen(De), and U. Sen, *Phys. Rev. Lett.* **90**, 100402 (2003)
13. M. Horodecki, P. Horodecki, R. Horodecki, J. Oppenheim, A. Sen(De), U. Sen, and B. Synak-Radtke, *Phys. Rev. A* **71**, 062307 (2005)
14. B.-L. Ye and S.-M. Fei, *Quantum Inf. Process.* **15**, 279 (2016)
15. S. Luo, *Phys. Rev. A* **77**, 042303 (2008)
16. M. Ali, A. R. P. Rau, and G. Alber, *Phys. Rev. A* **81**, 042105 (2010); Erratum in: *Phys. Rev. A* **82**, 069902(E) (2010)
17. X.-M. Lu, J. Ma, Z. Xi, and X. Wang, *Phys. Rev. A* **83**, 012327 (2011)
18. Q. Chen, C. Zhang, S. Yu, X. X. Yi, and C. H. Oh, *Phys. Rev. A* **84**, 042313 (2011)
19. X.-M. Lu, Z. Xi, Z. Sun, and X. Wang, *Quantum Inf. Comput.* **10**, 0994 (2010)
20. L. Ciliberti, R. Rossignoli, and N. Canosa, *Phys. Rev. A* **82**, 042316 (2010)

21. S. Vinjanampathy and A. R. P. Rau, J. Phys. A: Math. Theor. **45**, 095303 (2012)
22. N. Jing and B. Yu, J. Phys. A: Math. Theor. **49**, 385302 (2016)
23. Y. Huang, Phys. Rev. A **88**, 014302 (2013)
24. M. A. Yurischev, *Quantum discord for general X and CS states: a piecewise-analytical-numerical formula*, arXiv:1404.5735v1 [quant-ph]
25. M. A. Yurischev, J. Exp. Theor. Phys. **119**, 828 (2014); arXiv:1503.03316v1 [quant-ph]
26. M. A. Yurischev, Quantum Inf. Process. **14**, 3399 (2015)
27. M. A. Yurischev, Quantum Inf. Process. **16**:249 (2017); arXiv:1702.03728v3 [quant-ph]
28. B.-L. Ye, Y.-K. Wang, and S.-M. Fei, Int. J. Theor. Phys. **55**, 2237 (2016)
29. M. A. Yurischev, Quantum Inf. Process. **17**:6 (2018)
30. M. A. Yurischev, Quantum Inf. Process. **18**:124 (2019); arXiv:1804.03755v2 [quant-ph]
31. T. Chanda, T. Das, D. Sadhukhan, A. K. Pal, A. Sen(De), and U. Sen, Phys. Rev. A **92**, 062301 (2015)
32. T. Ray, H. K. Sing, A. Isaacs, and W. F. Smith, "Infeasibility driven evolutionary algorithm for constrained optimization". – In: *Constraint-handling in evolutionary optimization*, Edited by E. Mezura-Montes (Springer, Berlin 2009), pp. 145-165
33. M. G. Ivanov, *How to understand the quantum mechanics* (Regular and Chaotic Dynamics, Moscow-Izhevsk 2012), Sec. 5.3.2 [in Russian]
34. P. A. M. Dirac, *The principles of quantum mechanics* (Clarendon, Oxford 1930)
35. J. von Neumann, *Mathematische Grundlagen der Quantenmechanik* (Springer, Berlin 1932)
36. D. N. Zubarev, *Neravnovesnaya statisticheskaya termodinamika* (Nauka, Moskva 1971) [in Russian]
37. D. F. V. James, P. G. Kwiat, W. J. Munro, and A. G. White, Phys. Rev. A **64**, 052312 (2001)
38. C. Benedetti, A. P. Shurupov, M. G. A. Paris, G. Brida, and M. Genovese, Phys. Rev. A **87**, 052136 (2013)
39. N. A. Peters, J. B. Altepeter, D. Branning, E. Jeffrey, T.-C. Wei, and P. G. Kwiat, Phys. Rev. Lett. **92**, 133601 (2004); Erratum in: Phys. Rev. Lett. **96**, 159901 (2006)
40. M. Barbieri, F. De Martini, G. Di Nepi, and P. Mataloni, Phys. Rev. Lett. **92**, 177901 (2004)
41. A. Aiello, G. Puentes, D. Voigt, and J. P. Woerdman, Phys. Rev. A **75**, 062118 (2007)
42. F. Galve, G. L. Giorgi, and R. Zambrini, Phys. Rev. A **83**, 012102 (2011); Erratum in: Phys. Rev. A **83**, 069905(E) (2011)
43. R. Sun, X.-J. Ye, J.-S. Xu, X.-Y. Xu, J.-S. Tang, Y.-C. Wu, J.-L. Chen, C.-F. Li, and G.-C. Guo, Phys. Rev. Lett. **116**, 160404 (2016)
44. Yu. I. Bogdanov, K. G. Katamadze, G. V. Avosopiants, L. V. Belinsky, N. A. Bogdanova, A. A. Kalinkin, and S. P. Kulik, Phys. Rev. A **96**, 063803 (2017)
45. S. P. Kulik, G. A. Maslennikov, and E. V. Moreva, J. Exp. Theor. Phys. **105**, 712 (2006)
46. Yu. I. Bogdanov, E. V. Moreva, G. A. Maslennikov, R. F. Galeev, S. S. Straupe, and S. P. Kulik, Phys. Rev. A **73**, 063810 (2006)
47. J. Řeháček, B.-G. Englert, and D. Kaszlikowski, Phys. Rev. A **70**, 052321 (2004)
48. Yu. I. Bogdanov, G. Brida, M. Genovese, S. P. Kulik, E. V. Moreva, and A. P. Shurupov, Phys. Rev. Lett. **105**, 010404 (2010)
49. Yu. I. Bogdanov, G. Brida, I. D. Bukeev, M. Genovese, K. S. Kravtsov, S. P. Kulik, E. V. Moreva, A. A. Soloviev, and A. P. Shurupov, Phys. Rev. A **84**, 042108 (2011)
50. G. I. Struchalin, I. A. Pogorelov, S. S. Straupe, K. S. Kravtsov, I. V. Radchenko, and S. P. Kulik, Phys. Rev. A **93**, 012103 (2016)
51. S. S. Straupe, Pis'ma v ZhETF **104**, 540 (2016)
52. Yu. I. Bogdanov, J. Exp. Theor. Phys. **108**, 928 (2009)
53. Yu. I. Bogdanov, M. V. Chekhova, L. A. Krivitsky, S. P. Kulik, A. N. Penin, L. C. Kwek, A. A. Zhukov, C. H. Oh, and M. K. Tey, Phys. Rev. A **70**, 042303 (2004)
54. Yu. I. Bogdanov, *Statistical inverse problem: root approach*, arXiv:0312042v1 [quant-ph]
55. Yu. I. Bogdanov, L. A. Krivitsky, and S. P. Kulik, JETP Lett. **78**, 352 (2003)